since 1961

Baltica

BALTICA Volume 37 Number 1 June 2024: 39–46
https://doi.org/10.5200/baltica.2024.1.4

Investigation of the ground effects of Mw7.8 and Mw7.5 Maraş doublet earthquake on the south-east region (Bİtlİs-Zagros fold-thrust belt) of Turkey

Atınç Pırtı

Pirti, A. 2024. Investigation of the ground effects of Mw7.8 and Mw7.5 Maraş doublet earthquake on the south-east region (Bİtlİs-Zagros fold-thrust belt) of Turkey. *Baltica, 37 (1)*, 39–46. Vilnius. ISSN 1648-858X.
Manuscript submitted 27 February 2024 / Accepted 26 April 2024 / Available online 22 May 2024

Abstract. The Bitlis-Zagros Fold-Thrust Belt is one of the world's largest deformation zones, extending from the Eastern Mediterranean in southern Turkey to the south of Iran. This deformation zone is partitioned between different structures; however, little is known about the relative activities of these different structures and their effects on topography. The aim of this paper is to investigate the coseismic displacements resulting from the doublet earthquake that occurred in the vicinity of the city of Maraş (6 February 2023) by utilizing GNSS (Global Navigation Satellite System) stations (near the Bitlis-Zagros Fold-Thrust Belt) that are part of the CORS-TR (Continuously Operating Reference Station-Türkiye) geodetic network. After the doublet Maraş earthquake, south-westerly movements were observed at the ELAZ station, and south-east movements were observed at ERGN and MARD stations. As can be seen from the data obtained from these CORS-TR stations, the effect of the earthquake on the horizontal and vertical components was approximately 0.2–7.2 cm. These motions of ELAZ, ERGN and MARD stations can cause other earthquakes in the region of Bingöl, Van, Bitlis and Muş in the future.

Keywords*: Maraş Earthquakes 2023; displacement; deformation; accuracy; precision*

Atınç Pirti (atinc@yildiz.edu.tr), http://orcid.org/0000-0001-9197-3411
Department of Geomatics Engineering, Yildiz Technical University, 34220 Esenler, Istanbul – Turkiye

INTRODUCTION

After a doublet earthquake, like the M7.8 and M7.5 *Maraş Earthquake Sequence*, it is extremely common for hundreds of aftershocks to occur over the next few weeks, months, or possibly years. Eventually, the frequency of these aftershocks will decrease. Aftershocks are not always restricted to the same fault system as the mainshock, as large quakes can sometimes trigger aftershocks further away. The Bitlis-Zagros Fold-Thrust Belt (BZFTB) formed as a result of the collision between the Eurasian and the Arabian Plates and closing of the Neotethys Ocean (Dewey *et al*. 1986). The BZFTB is part of the Alpine-Himalayan orogenic belt, which extends in the E-W direction starting from the eastern Mediterranean and extending eastwards about 2000 km (Dewey *et al*. 1973; Dercourt *et al*. 1986; Stampfli, Borel 2002; Mouthereau *et al*. 2012). The BZFTB at the eastern end of the Mediterranean extends eastwards approximately 650 km with a convex curve towards the north and ends at the north-eastern Zagros Şemdinli-Yüksekova Fault Zone. These significant translational fault networks cover a significant portion of central and western Turkey and allow the Anatolian block to move to the west as it is pressed by the convergent Arabian and Eurasian plates. The Bitlis Suture Zone (in eastern Turkey) and the Zagros fold and thrust belt (toward Iran) are the main tectonic features in the region around Lake Van and farther east. Beyond the eastern border of the Anatolian strike-slip tectonics, there was a vast zone of convergence where the 23 October 2011 earthquake struck (Nicoll 2010; Mouthereau *et al*. 2012). The BZFTB is subdivided into four NW-trending tectonic zones from northeast to southwest and major faults form the boundaries of each tectonic zone (Jassim, Goff 2006). The NW–SE trending Zagros Orogen Belt is divided into

subtectonic units. The length of BZFTB within the borders of Turkey (Maraş-Hakkâri) exceeds 650 km. The faults in the eastern part of the BZFTB in Turkey, where the zone expands over a wide area, were named as the Hakkâri and Şirvan Segments (Emre *et al*. 2013). The Şirvan Segment starts in the northeast of central Siirt and extends for 60 km towards the east in the direction of N 70°–85°W. It is seen that the Şirvan Fault has a right lateral component in some areas along its length. The Hakkâri Segment extends for 19 km with a direction of N 85°W and consists of faults developed in a braided pattern in the region. The other main deformation structures in the BZFTB are folds. The main directions of the folds along the suture zone vary; the majority of the folds that remain on the borders of Turkey trend N–S or N 10–°W and dip towards the north; however, these folds trend N 60–70°W in the Iraq region (Abdulnaby *et al*. 2021; Afsari *et al*. 2011). The Bitlis-Zagros Fold-Thrust Belt is one of the most seismically active regions among the present active belts (Tatar *et al*. 2004). The Zagros fold-thrust belt is famous among geologists and is one of the most-studied terrains in the world. Because of its unique structures, the Zagros orogeny is challenging for many researchers and experts (Tatar *et al*. 2004; Dewey *et al*. 1973; Dercourt *et al*. 1986; Stampfli, Borel 2002; Mouthereau *et al*. 2012; Jassim, Goff (2006)).

The aim of this paper is to examine the coseismic displacements of GNSS stations (near the Bitlis-Zagros Fold-Thrust Belt) that are part of the CORS-TR geodetic network after the double earthquake of Maraş that occurred in the vicinity of the city of Maraş (6 February 2023).

MATERIALS AND METHODS

Trimble CenterPoint RTX GNSS processing software

The Trimble RTX service utilized in this research may be accessed at https://trimblertx.com/. The service makes it possible to submit GNSS observation data to the system and obtain coordinate information as a report. For data acquired before 23 March 2017, position computations are performed by using the ITRF2008 (International Terrestrial Reference Frame) datum, while for data gathered after 23 March 2017, they are made using the ITRF2014 (International Terrestrial Reference Frame) datum. Additionally, it gives the user a choice of tectonic plates and a different coordinate system. The service accepts observation files in the RINEX 2.x, RINEX 3.x, Trimble T01, T02, and DAT formats. A minimum of 60 minutes and a maximum of 24 hours should be included in observation files. Only static data files should be used. Dual frequency coding and carrier phase observations (L1 and L2) should also be included. Less than two minutes after the observation files are submitted to the system, the findings are provided to the email address. The Center Point RTX post-processing service allows the transformation of the current epoch ITRF2008 / ITRF2014 position to another reference frame with a different reference epoch and based on a selected tectonic plate. If the user is not using the current epoch of ITRF2008 / ITRF2014 and is not sure which plate they're on, it is recommended to select (Auto-detect) for the tectonic plate setting. The achievable accuracy level of the Center Point RTX post-processing service is 2 cm or better in the horizontal and approximately 6 cm in the vertical. This is based on a minimum 1-hour observation file. As the data session approaches, but does not exceed 24 hours, accuracy can approach 1 cm in the horizontal and 3 cm in the vertical (Trimble 2023).

Static GNSS method

To determine high-precision three-dimensional coordinates at traverse stations, GNSS surveying using the static method is often preferred. These systems offer coordinates of ground sites at a millimetre level in both the horizontal and vertical components. Additionally, precise azimuth determination is made possible by the static GNSS method, allowing for the establishment of the network's orientation in relation to the reference system. When compared to networks observed with electromagnetic distance measuring devices, surveying networks with GNSS positioning have the advantage of not requiring inter-visibility and are more robust against geodynamic phenomena like polar motion, Earth tides, and crustal motion (Jackson, Kagan 2011; Ghilani, Wolf 2012; Gonzales 2009; Hoffman *et al*. 2008).

Study site

The Bitlis-Zagros Fold-Thrust Belt, which stretches from Turkey and Iraq in the north to the Strait of Hormuz in the south, was created as a consequence of collision. According to geological data, the Bitlis-Zagros Fold-Thrust Belt experienced a number of tectonic events that had an impact on diverse regions of the belt. Among the currently active belts, the Bitlis-Zagros Fold-Thrust Belt is one of the seismically active zones (Tatar *et al*. 2004). There are two main tendencies in the Bitlis-Zagros Fold-Thrust Belt: the E–W Bitlis Trend between the Arabian and Anatolian plates and the NW–SE Zagros Trend between the Arabian and Iranian plates. The curvature of the northern Arabian Plate edge determines the curved form of this mountain belt's trend. The Anatolian

Plate is experiencing a space issue as a result of the Arabian Plate colliding with it. The Turkish Plate is thus shifting laterally to the west along two significant conjugate strike-slip faults that penetrate the Earth's crust. According to Abdulnaby *et al*. (2021) and Afsari *et al*. (2011), the East Anatolian Fault (EAF) and North Anatolian Fault (NAF) are to blame for some of Turkey's most deadly earthquakes (Fig. 1).

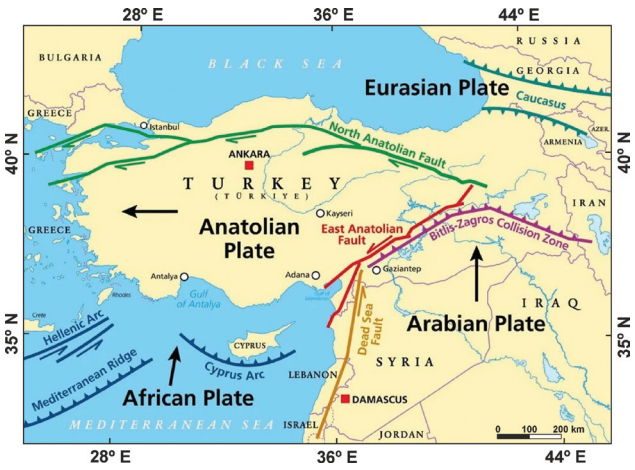

Fig. 1 Bitlis-Zagros Collision Zone and other plates in Turkey

RESULTS

In order to totally understand the magnitudes of the displacements brought on by the Maraş doublet earthquake in Pazarcık and Elbistan, the data of CORS-TR stations near the earthquake epicentre is quite useful. These stations in the CORS-TR network (Fig. 2) record data at 1-second intervals, which makes them especially useful for examining earthquakes and crustal deformations. The CORS-TR server provided a 24-hour RINEX observation file with 1/30-second interval (Receiver Independence Exchange). The 24-hour RINEX observation file was obtained from these stations processed and analysed by using the Trimble CenterPoint RTX GNSS post-processing software (static (24 hours) – record interval: 1/30 second). Static processing results were derived from the static solutions (24 hours) by computing the ITRF 2014 Epoch with 2023.1 coordinates with horizontal accuracy of 2–6 mm and 6–11 mm in vertical coordinates before the two earthquakes period (05 05 2023), (Table 1).

The data of 6 February 2023 were processed and analysed by using the Trimble Center Point RTX GNSS post-processing software (static method, 1-second interval) to examine the earth-

Table 1 Standard deviations and ITRF14 (2023.1 Epoch) coordinates of six CORS-TR stations near the region of the Maraş doublet earthquake on 05 02 2023

Station	Latitude (φ)	Longitude (λ)	Altitude (h) [m]	Std (φ) [mm]	Std (λ) [mm]	Std (h) [mm]
ELAZ	38°38'40.83240"	39°15'23.28191"	1027,382	2	3	6
ERGN	38°16'10.59042"	39°45'29.50834"	987,868	3	5	11
HAK1	37°34'34.15862"	43°44'2.46854"	1773,275	3	4	7
MARD	37°18'37.81732"	40°43'41.84458"	1064,181	2	4	8
SEM1	37°18'21.30428"	44°34'22.17913"	1413.792	2	4	8
SRT1	37°56'17.10932"	41°55'25.57331"	925,596	4	6	11

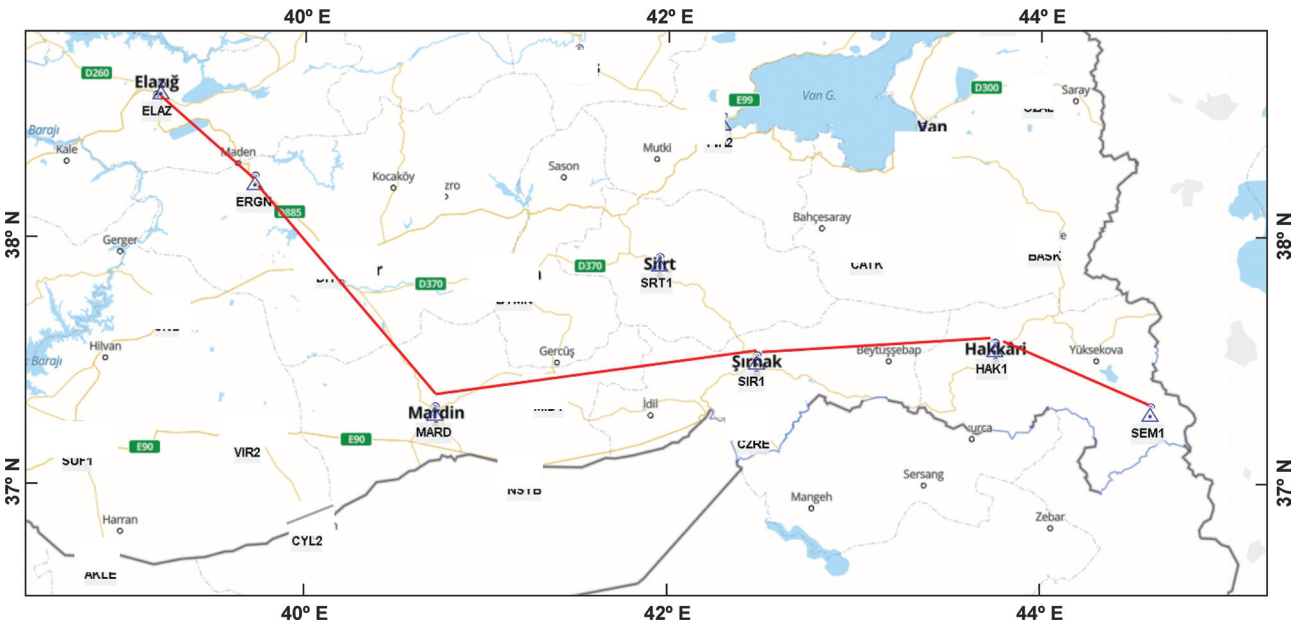

Fig. 2 CORS-TR stations in the study region (Bitlis-Zagros Fold and Thrust Belt)

quake impacts that may be seen. The coordinates of six CORS-TR stations (05 05 2023) obtained by processing the static method were compared with the coordinates (06 02 2023) obtained by using the static method. Figures 3, 4, 5, 6, 7, and 8 show how the Maraş-centred doublet earthquake impacted these CORS-TR stations (compute the obtained coordinate differences).

Figure 3a shows the discrepancies in ELAZ station's horizontal and vertical components. The position of the ELAZ station before the first earthquake, during the first and second doublet earthquake, as well as its instantaneous vector motions, are shown in Fig. 3a. Two earthquakes' positions and vector motions are shown in three dimensions in Fig. 3b. Figures 3a and 3b illustrate where the ELAZ point was on 5 February 2023 (blue circle), where it was on 6 February 2023, during the first earthquake (red circle), and where it was on 6 February 2023, during the second earthquake (black circle). At the ELAZ station (Fig. 3a), the horizontal displacement computed before/after the first earthquake was totally 4.3 cm in the south-west direction, whereas the horizontal displacement calculated after the second earthquake was totally 2.9 cm in the south-west direction. The total horizontal displacements after two earthquakes were computed to be 7.2 cm in the south-west direction. At the ELAZ station, the swelling movement in height values was observed at 1–1.9 cm after two earthquakes.

Figure 4a depicts the differences in ERGN station's horizontal and vertical components. The posi-

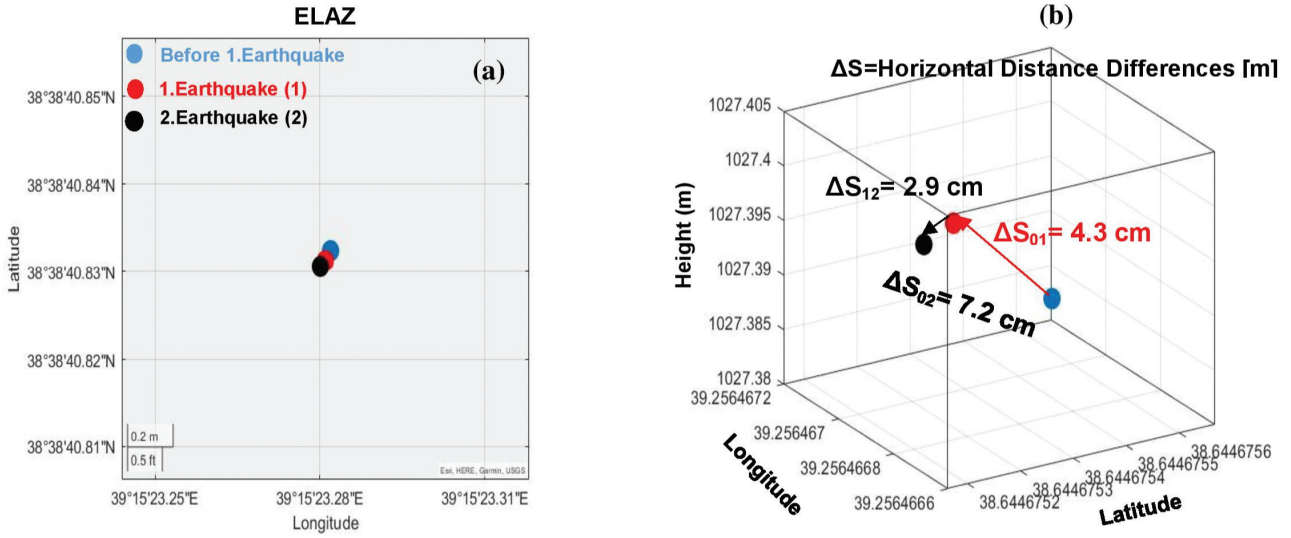

Fig. 3 (a) Horizontal displacements of ELAZ station before/during doublet earthquake in the study region by using static GNSS method (05 02 2023–06 02 2023); (b) 3D displacements of ELAZ station and Horizontal Distances Differences (ΔS**)** among the earthquakes

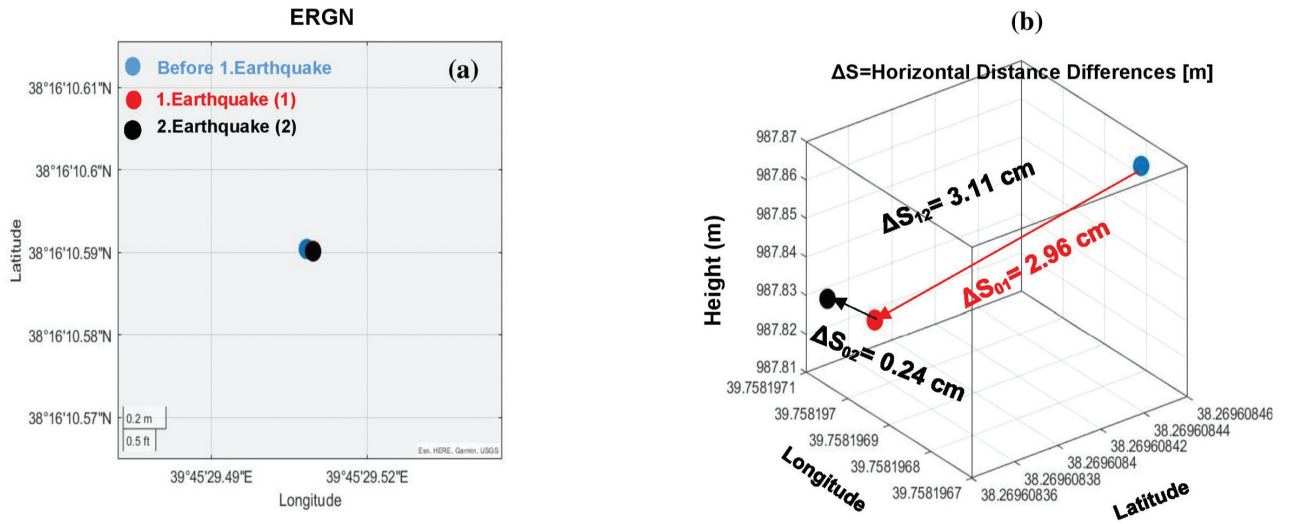

Fig. 4 (a) Horizontal displacements of ERGN station before/during two earthquakes in the study region by using static GNSS method (05 02 2023–06 02 2023); (b) 3D displacements of ERGN station and Horizontal Distances Differences (ΔS**)** among the earthquakes

tion of the ERGN station before the first earthquake, during the first and second earthquakes, as well as its instantaneous vector motions, are illustrated in Fig. 4a. Two earthquakes' positions and vector motions are shown in three dimensions in Fig. 4b. Figures 4a and 4b show where the ERGN point was on 5 February 2023 (blue circle), where it was on 6 February 2023, during the first earthquake (red circle), and where it was on 6 February 2023, during the second earthquake (black circle). At the ERGN station (Fig. 4a), the horizontal displacement computed before/after the first earthquake was 2.96 cm in the north-east direction, whereas the horizontal displacement computed after the second earthquake was 0.24 cm in the south-east direction. The total horizontal displacements of 3.11 cm in the north-east direction were obtained. At the ERGN station, collapse movements in height values were observed at 4–5 cm after two earthquakes (Fig. 4b).

Figure 5a illustrates the discrepancies in the HAK1 station's horizontal and vertical components. The position of the HAK1 station before the first earthquake, during the first and second earthquakes, as well as its instantaneous vector motions, are shown in Fig. 5a. Two earthquakes' positions and vector motions are shown in three dimensions in Fig. 5b. Figures 5a and 5b show where the HAK1 point was on 5 February 2023 (blue circle), where it was on 6 February 2023, during the first earthquake (red circle), and where it was on 6 February 2023, during the second earthquake

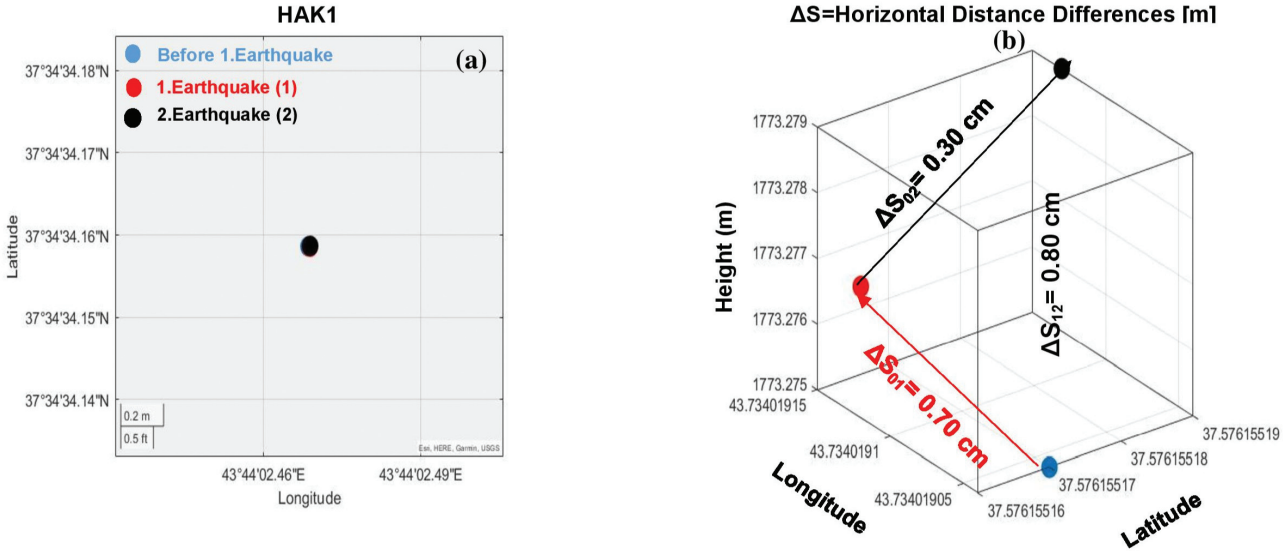

Fig. 5 (a) Horizontal displacements of HAK1 station before/during two earthquakes in the study region by using static GNSS method (05 02 2023–06 02 2023); (b) 3D displacements of HAK1 station and Horizontal Distances Differences (ΔS**)** among the earthquakes

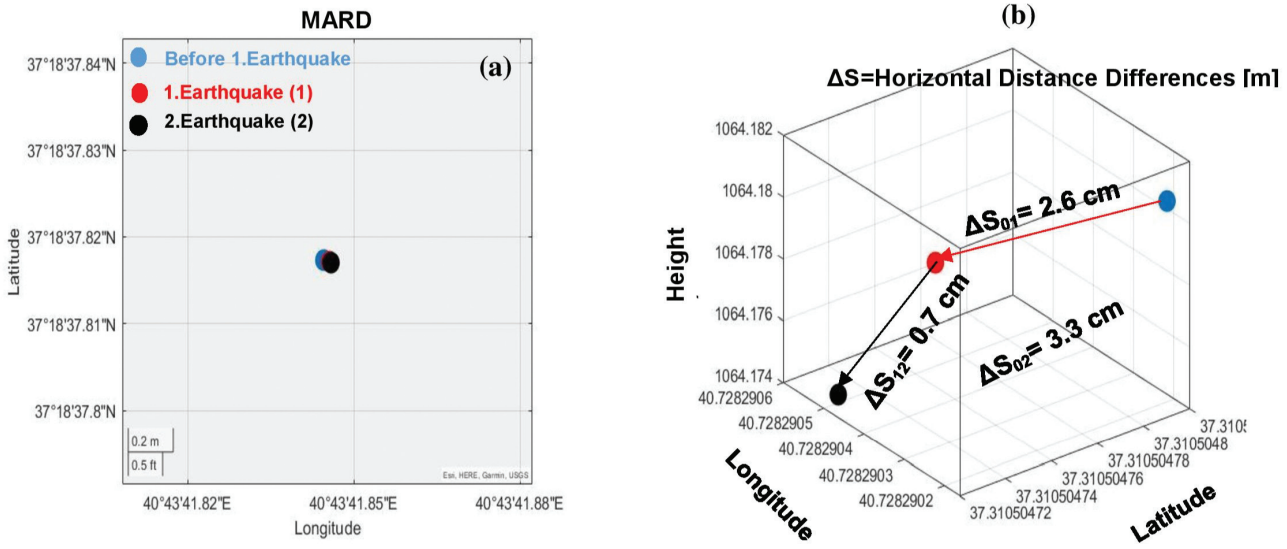

Fig. 6 (a) Horizontal displacements of MARD station before/during two earthquakes in the study region by using static GNSS method (05 02 2023–06 02 2023); (b) 3D displacements of MARD station and Horizontal Distances Differences (ΔS) among the earthquakes

(black circle). At the HAK1 station (Fig. 5a), the horizontal displacement computed before/after the first earthquake was 0.70 cm in the south-east direction, whereas the horizontal displacement calculated after the second earthquake was 0.30 cm in the west direction. The total horizontal displacements of 0.80 cm in the west direction were gained. At the HAK1 station, swelling movements in height values were observed at 0.2–0.4 cm after two earthquakes, see Fig. 5b.

Figure 6a shows the discrepancies in MARD station's horizontal and vertical components. The position of the MARD station before the first earthquake, during the first and second earthquakes, as well as its instantaneous vector motions, are shown in Fig. 6a. Two earthquakes' positions and vector motions are shown in three dimensions in Fig. 6b. Figures 6a and 6b show where the MARD point was on 5 February 2023 (blue circle), where it was on 6 February 2023, during the first earthquake (red circle), and where it was on 6 February 2023, during the second earthquake (black circle). At the MARD station (Fig. 6b), the horizontal displacement computed after the first earthquake was 2.6 cm in the north-east direction, whereas the horizontal displacement calculated after the second earthquake was 0.7 cm in the south-east direction. The total horizontal displacements were 3.3 cm in the north-east direction. At the MARD station, collapse movements in height values were observed at 0.3–0.7 cm after two earthquakes, see Fig. 6b.

Figure 7a illustrates the discrepancies in SEM1 station's horizontal and vertical components. The position of the SEM1 station before the first earthquake, during the first and second earthquakes, as well as its instantaneous vector motions, are shown in Fig. 7a.

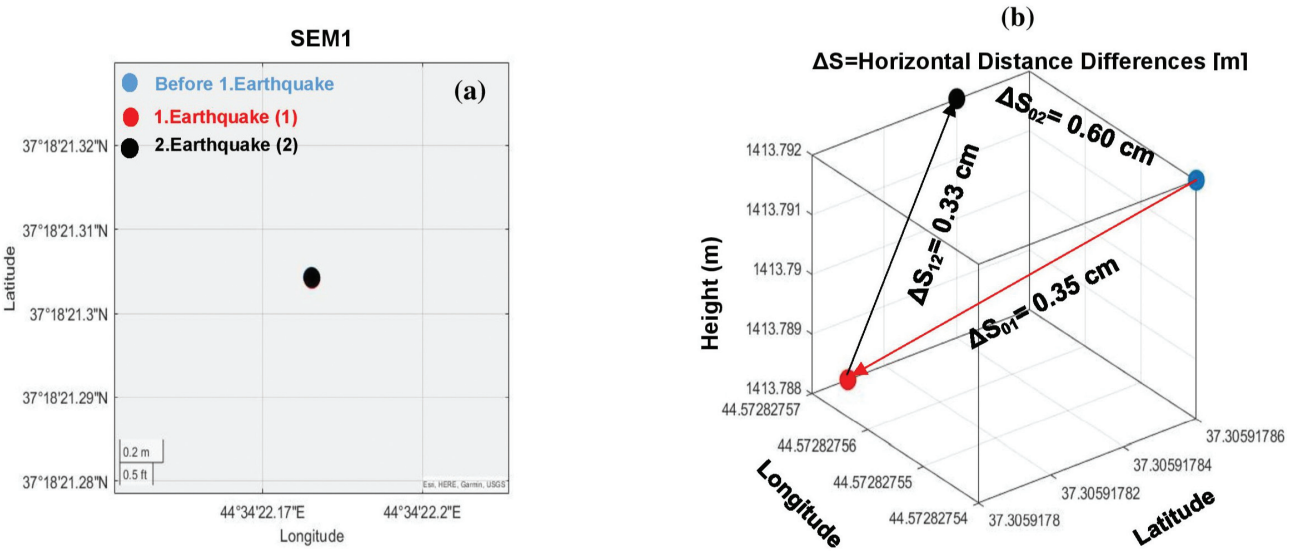

Fig. 7 (a) Horizontal displacements of SEM1 station before/during two earthquakes in the study region by using static GNSS method (05 02 2023–06 02 2023); (b) 3D displacements of SEM1 station and Horizontal Distances Differences (ΔS) among the earthquakes

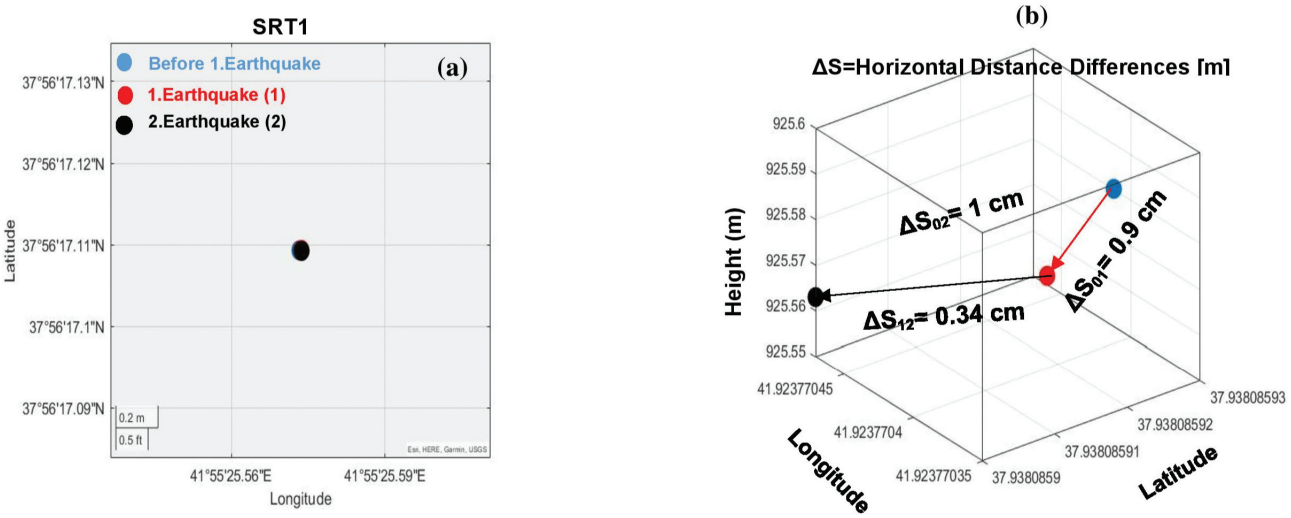

Fig. 8 (a) Horizontal displacements of SRT1 stations before/during two earthquakes in the study region by using static GNSS method (05 02 2023–06 02 2023); (b) 3D displacements of SRT1 station and Distances Differences (ΔS) among the earthquakes

Two earthquakes' positions and vector motions are shown in three dimensions in Fig. 7b. Figures 6a and 6b show where the SEM1 point was on 5 February 2023 (blue circle), where it was on 6 February 2023, during the first earthquake (red circle), and where it was on 6 February 2023, during the second earthquake (black circle). At the SEM1 station (Fig. 7a), the horizontal displacement computed after the first earthquake was 0.35 cm in the south-west direction, whereas the horizontal displacement calculated after the second earthquake was 0.33 cm in the south-west direction. The total horizontal displacements were computed to be 0.68 cm in the south-west direction. At the SEM1 station, collapsing-swelling movements in height values were observed at 0.2–0.4 cm after two earthquakes.

Figure 8a displays the discrepancies in SRT1 station's horizontal and vertical coordinates. The locations of the SRT1 station before the first earthquake, during the first and second earthquakes, as well as its instantaneous vector motions, are shown in Fig. 8a. Two earthquakes' positions and vector motions are shown in three dimensions in Fig. 8b. Figures 8a and 8b depict where the SRT1 point was on 5 February 2023 (blue circle), where it was on 6 February 2023, during the first earthquake (red circle), and where it was on 6 February 2023, during the second earthquake (black circle). At the SRT1 station (Fig. 8a), the horizontal displacement computed after the first earthquake was 0.9 cm in the south-west direction, whereas the horizontal displacement computed after the second earthquake was 0.34 cm in the north-west direction. The total horizontal displacements were calculated to be 1 cm in the north-west direction. At the SRT1 station, collapsing movements in height values were observed at 3.3–4.4 cm after two earthquakes, see Fig. 8b.

DISCUSSION

The Bitlis-Zagros Fold-Thrust Belt is one of the world's largest deformation zones, extending from the Eastern Mediterranean in southern Turkey to the south of Iran. This deformation zone is partitioned between different structures; however, little is known about the relative activities of these different structures and their effects on topography. It is clearly understood that the earthquakes in Turkey were caused by the collision of the Arabian plateau and Anatolia in the Bitlis Thrust Zone, which arcs in the southeast. The horizontal and vertical displacements (coseismic) caused by the 6 February 2023 Maraş double earthquake were effectively determined by using the static GNSS processing method. For this reason, CORS-TR stations close to the Bitlis-Zagros Fold-Thrust Belt were selected. Using GNSS data of these stations by using the static method, horizontal and vertical displacements were successfully computed with cm accuracy. The biggest horizontal displacement value was obtained at the ELAZ station, which is about 200–255 kilometres from the epicentres of two earthquakes. This horizontal displacement value was 7.2 cm in the west direction for the ELAZ station. As can be seen from the data obtained from these CORS-TR stations, the effect of the earthquake on the horizontal and vertical components was approximately 0.2–7.2 cm. Elazığ is a settlement centre located on the Eastern Anatolian Fault Line, where the earthquake risk is the highest. Elazığ is surrounded by active faults on all sides. It is obvious that Elazığ city centre is covered with alluvial soils and the buildings in the region are at high earthquake risk.

CONCLUSIONS

After the Maraş doublet earthquake, south-westerly movements were observed at the ELAZ station, and south-east movements were observed at ERGN and MARD stations. These motions of ELAZ, ERGN and MARD stations can cause other earthquakes in the region of Bingöl, Van, Bitlis and Muş in the future (When the EAF produced the 6 February earthquakes, it may have transferred some energy – possibly as much as 20 percent – to this Bitlis-Zagros thrust zone. This means that new earthquakes may occur, especially in the cities between Adıyaman and Hakkari, with the activation of the Bitlis-Zagros belt). Northern Iraq represents part of the convergent plate boundary between the Arabian and Eurasian plates. The collision zone between these two plates is manifested by the Bitlis-Zagros Fold-Thrust Belt. This belt is one of the most seismically active regions among the present active belts.

ACKNOWLEDGEMENTS

I thank anonymous reviewers for their suggestions and corrections.

REFERENCES

Abdulnaby, W., Mahdi, H., Al-Shukri, H. 2012.*Crustal structure from joint inversion of receiver function and surface wave dispersion beneath Duhok, NW Iraq*. Istanbul International Geophysical Conference and Oil and Gas Exhibition, Istanbul, Turkey, 17–19 September 2012.

Afsari, N., Sodoudi, F., Taghizadeh, F., Reza, G.M. 2011. Crustal structure of Northwest Zagrs (Kermanshah) and Central Iran (Yazd and Isfahan) Using Teleseismic Ps Converted Phase. *Journal of Seismology 15*, 341–353.

Dercourt, J. et al. 1986. Geological Evolution of the Tethys Belt from the Atlantic to the Pamirs since the Lias. *Tectonophysics 123*, 241–315. https://doi.org/10.1016/0040-1951(86)90199-X

Dewey, J.F., Pitman, W., Ryan, W., Bonin, J. 1973. Plate Tectonics and the Evolution of the Alpine System. *Geological Society of America Bulletin 84*, 3137–3180. http://dx.doi.org/10.1130/0016-7606-(1973)84<3137:PTATEO>2.0.CO;2

Dewey J.F., Hempton M.R., Kidd W.S.F., Şaroğlu F., Şengör A.M.C. 1986. Shortening of Continental Lithosphere: the Neotectonics of Eastern Anatolia-a Young Collision Zone. *Geological Society, London, Special Publications 19*, 1–36. https://doi.org/10.1144/GSL.SP.1986.019.01.01

Emre, Ö., Duman, T.Y., Özalp, S., Elmacı, H., Olgun, Ş., Şaroğlu, F. 2013. *Active Fault Map of Turkey with an Explanatory Text. 1:1,250,000 Scale*. General Directorate of Mineral Research and Exploration, Ankara, 2013.

González, A. 2009. *Sistema de Posicionamiento Global (GPS)*. Editorial Escuela Colombiana de Ingeniería.

Hofmann, B., Lichtenegger, H., Wasle, E. 2008. *Global Navigation Satellite Systems: GPS, GLONASS, Galileo and more*. Wien, Austria: Springer-Verlag Berlin Heidelberg.

Jackson, D.D., Kagan, Y.Y. 2011. Characteristic Earthquakes and Seismic Gaps. In: *Encyclopedia of Solid Earth Geophysics 5*, 1539. DOI: 10.1007/978-90-481-8702-7.

Jassim, S.Z., Goff, J.C. 2006. *Geology of Iraq*. 1st Edition, Published by Dolin, Prague and Moravian Museum, Brno, Czech Republic.

Mouthereau, F., Lacombe, O., Vergés, J. 2012. Building the Zagros collisional orogen: Timing, strain distribution and the dynamics of Arabia/Eurasia plate convergence. *Tectonophysics 532–535 (4)*, 27–60. https://doi.org/10.1016/j.tecto.2012.01.022

Nicoll, K. 2010. Landscape development within a young collision zone: implications for post-Tethyan evolution of the Upper Tigris River system in southeastern Turkey. *International Geology Review – Int geol rev 52*. https://doi.org/10.1080/00206810902951072.

Stampfli, G.M., Borel, G.D. 2002. A Plate Tectonic Model for the Paleozoic and Mesozoic Constrained by Dynamic Plate Boundaries and Restored Synthetic Oceanic Isochrons. *Earth and Planetary Science Letters 196*, 17–33. http://dx.doi.org/10.1016/S0012-821X(01)00588-X

Tatar, M., Hatzfeld, D., Ghafori-Ashtiany, M. 2004. Tectonics of the Central Zagros (Iran) deduced from microearthquake seismicity. *Geophysical Journal International 156*, 255–266.

Internet sources:

Ghilani, C. D., Wolf, P. R. 2012. *Elementary Surveying: An Introduction to Geomatics* (13th Edition). Vasa. Prentice Hall. Retrieved from http://medcontent.metapress.com/index/A65RM03P4874243N.pdf%5Cn http://www.getcited.org/pub/102714699

Trimble 2023. Trimble Center Point RTX Post-processing Software, http://trl.trimble.com/docushare/dsweb/Get/Document-792295/TAP201606-0017-FAQ%20-%20Frequently%20Asked%20Questions%20-20Trimble%20CenterPoint%20RTX%20Post-Processing.pdf